Justine Rey
Undergraduate Student
e-mail: justinerey.1@gmail.com

Matthieu Vandamme[1]
Assistant Professor
e-mail: matthieu.vandamme@enpc.fr

Laboratoire Navier (École des Ponts ParisTech/
IFSTTAR/CNRS),
École des Ponts ParisTech,
Université Paris-Est,
77420 Champs-sur-Marne, France

On the Shrinkage and Stiffening of a Cellulose Sponge Upon Drying

Everyone can observe the peculiar effect of water on a sponge: upon drying, a sponge shrinks and stiffens; it swells and softens upon wetting. In this work, we aim to explain and model this behavior by using the Biot–Coussy poromechanical framework. We measure the volume and the bulk modulus of sponges at different water contents. Upon drying, the volume of the sponge decreases by more than half and its bulk modulus increases by almost two orders of magnitude. We develop a partially saturated microporomechanical model of the sponge undergoing finite transformations. The model compares well with the experimental data. We show that about half of the stiffening of the sponge upon drying is due to geometrical nonlinearities induced by a closing of the pores under the action of capillary pressure. The other half of the stiffening can be explained by the nonlinear elastic properties of the cellulose material itself. [DOI: 10.1115/1.4007906]

1 Introduction

A kitchen sponge is a common object of daily use. Nevertheless, its behavior can be surprising: a wet sponge left overnight beside the sink will be shrunken and hard in the morning. When immersed in water, the same sponge will swell back and soften tremendously. Such a peculiar response to an intake of water is also observed for other natural or man-made materials: soil, concrete, bread, etc.

Most kitchen sponges are made of cellulose. Cellulose is the most abundant organic compound on Earth [1]. It is a naturally occurring polymer, which is the main constituent of plants. In industry, cellulose is mostly used to produce paper or paperboard.

Cellulose is a polysaccharide composed of β-D-glucopyranose units linked by glycosidic bonds [2]. The degree of polymerization of cellulose found in nature can be greater than ten thousand [3]. Despite decades of intensive research, the exact structure of cellulose still remains unresolved. Cellulose can exist in more or less crystalline forms and at least six different polymorphs of its crystalline structure have already been identified [1]. Due to the presence of hydroxyl groups and oxygen atoms, there exists a significant amount of hydrogen bonds within a cellulose chain, and between neighboring chains: those hydrogen bonds play a significant role in the structure and on the mechanical properties of cellulosic materials [4–7].

When immersed in water, cellulose swells [8]. This swelling depends on the chemistry of the surrounding fluid [9–11]. The surrounding liquid also has an effect on the mechanical properties of the cellulose [12]. In the presence of moisture, the intake of water depends on the structure of the hydrogen bonds [13]. Moisture has an effect on the mechanical properties of cellulose [14–16].

At the structural level, sponge is a porous material. In a manner similar to any porous material, upon drying, water will leave the pores and the material will become partially saturated. For surface energy reasons (for an in-depth explanation, see, for instance, Ref. [17]), at equilibrium at a given relative humidity, the larger pores will be empty (full of air), while the smaller pores will still be saturated with liquid water. The lower the relative humidity, the smaller the critical radius below which pores remain saturated. Liquid water can be in thermodynamic equilibrium with air with a relative humidity below 100% only if the pressure in the liquid water drops below that of the surrounding air. The drier the air, the greater the drop in the pressure of the liquid water. This depressed water will pull on the saturated pores and, thus, lead to a global shrinkage of the material. The same mechanism contributes, for instance, to the drying shrinkage of concrete [18]. In this work, we aim to determine whether the same mechanism can explain why a sponge shrinks and stiffens upon drying. In other words, can the mechanical behavior of a cellulose sponge upon drying be explained and modeled by considering it as a regular partially saturated porous solid?

Our study begins with an experimental campaign of measurements of the shrinkage and stiffening of a cellulose sponge at several stages of the drying process. We then develop a partially saturated poromechanical model of a sponge in finite transformations. In a later section, the developed model is compared with the experimental data and the results are discussed.

2 Experimental Study of the Effect of Water on the Volume and on the Elastic Properties of a Sponge

In this section, we present the experimental study we performed in order to characterize the effect of drying on the volume and the elastic properties of a cellulose sponge.

2.1 Materials and Methods. The experimental study was performed on four parallelepipedic Nicols heavy-duty sponges. Their dry mass, measured after oven drying, was $23.7\text{g} \pm 5.6\%$. Their volume upon full wetting was $744\text{cm}^3 \pm 2.3\%$. The small coefficients of variation suggest that the four sponges were similar.

We performed measurements of the volume and elastic properties at various drying stages. The sponges were first completely wet. After each measurement, we dried them with a hairdryer. We then hermetically wrapped them with silver foil and waited half a day so that the remaining water diffused and was uniformly distributed in the sponge.

At each stage of the drying process, the mass of the sponges was measured with a balance with an accuracy of 0.01 g. Upon drying, the sponges remained reasonably parallelepipedic: their dimensions, and thus their volume, were measured with a caliper. Then the bulk modulus of the sponges was measured. In order to do so, we performed compression tests in each of the three principal directions of the sponge with an MTS tensile/compression machine. A ramp displacement was applied at a velocity of

[1]Corresponding author.

Manuscript received December 24, 2010; final manuscript received April 11, 2012; accepted manuscript posted October 25, 2012; published online February 6, 2013. Assoc. Editor: Younane Abousleiman.

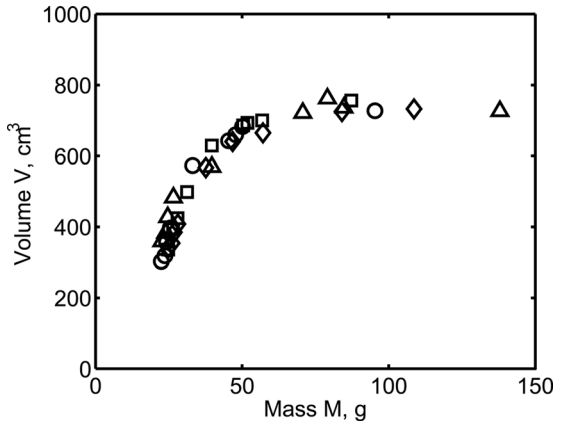

Fig. 1 Volume *V* of the sponge versus its mass *M*. Different symbols represent different sponges.

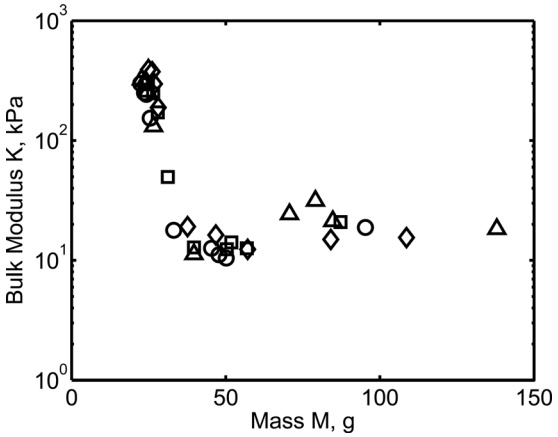

Fig. 2 Bulk modulus *K* of the sponge versus its mass *M*. Different symbols represent different sponges.

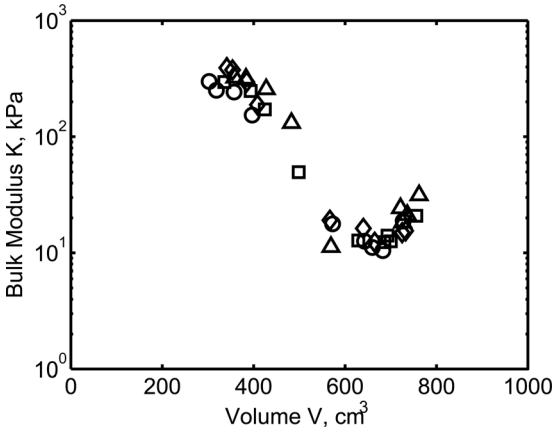

Fig. 3 Bulk modulus *K* of the sponge versus its volume *V*. Different symbols represent different sponges.

5 mm.min^{-1}. The force was measured with an accuracy of 0.01 N. The acquisition rate was 10 Hz. Each compression test provided the Young's modulus E_i in the ith principal direction of the sponge. The bulk modulus K of the sponge was then calculated by using

$$K^{-1} = (1 - 2\nu)\sum E_i^{-1} \tag{1}$$

where ν is the Poisson's ratio and where we assumed $\nu = 0.25$. This assumed value for ν was checked *a posteriori* (see Sec. 4.2).

2.2 Results. Upon drying, the sponge lost water and its mass decreased. We display in Fig. 1 the volume V of the sponge versus its mass M. As is intuitively expected, the drier the sponge was, the more it shrank. From a totally wet state to an asymptotically dry state, the volume of the sponge decreased by more than 50%.

Different stages can clearly be distinguished. At high water contents ($M > 70$ g), the volume of the sponge was mostly insensitive to the water content. At medium water contents ($30\text{ g} < M < 70\text{ g}$), the volume started decreasing more and more significantly with a loss of water. At the lowest water contents ($M < 30$ g), the volume decreased very significantly with additional drying and the volume of the sponge scaled almost linearly with its mass.

We display in Figs. 2 and 3 the bulk modulus K of the sponge versus its mass M and its volume V, respectively. From the softest state to the stiffest state, the bulk modulus of the sponge increased by about one and a half orders of magnitude. Surprisingly, at high water contents ($M > 70$ g), the sponge became softer upon drying. This somewhat counterintuitive result might be an experimental artifact: at such high saturations, some water might be squeezed out of the sponge during the compression test. It might be that, because of the duration of this consolidation process, the compression experiments were not performed in fully drained conditions; thus providing higher apparent elastic properties. At medium water contents ($30\text{ g} < M < 70\text{ g}$), the bulk modulus increased slightly upon drying. At the lowest water contents ($M < 30$ g), the bulk modulus increased more significantly with additional drying.

3 Derivation of a Poromechanical Model for a Sponge

We aim to develop a model that captures the response (the variation of the volume and the bulk modulus) of the cellulose sponge to an intake or to a loss of water. Since a sponge is porous, we propose to develop the model in the Biot–Coussy poromechanical framework [17,19]. To capture the fact that some pores are saturated with liquid water while others are full of air, the model will be partially saturated. Since the deformations induced by drying can be tremendous, the model will be derived in finite transformations. We will assume, however, that the solid matrix of the sponge (the cellulose material itself) behaves in a linear elastic manner.

3.1 Basic Poroelastic Equations. The development of the model starts from the usual partially saturated poroelastic state equations [17]

$$d\sigma = K d\varepsilon - b_L dp_L - b_G dp_G \tag{2}$$

$$d\varphi_L = b_L d\varepsilon + \frac{dp_L}{N_{LL}} + \frac{dp_G}{N_{LG}} \tag{3}$$

$$d\varphi_G = b_G d\varepsilon + \frac{dp_L}{N_{LG}} + \frac{dp_G}{N_{GG}} \tag{4}$$

where σ is the confining stress, ε is the volumetric strain, p_L is the pressure of the liquid phase (water), p_G is the pressure of the gas phase (air), p_{atm} is the reference atmospheric pressure, φ_L is the variation of the porosity occupied by the liquid phase, φ_G is the variation of the porosity occupied by the gas phase, b_L and b_G are the Biot coefficients, and N_{LL}, N_{LG}, and N_{GG} are the Biot moduli. The state of reference is when the pore space is at atmospheric pressure. In the preceding state equations, all variables are Lagrangian variables, i.e., are defined with respect to the state of reference. There exist classical relations on the poroelastic parameters [17]

$$b_L + b_G = 1 - \frac{K}{K_S} \tag{5}$$

$$\frac{1}{N_{LL}} + \frac{1}{N_{LG}} = \frac{b_L - \phi_L}{K_S} \tag{6}$$

$$\frac{1}{N_{GG}} + \frac{1}{N_{LG}} = \frac{b_G - \phi_G}{K_S} \tag{7}$$

where K_S is the bulk modulus of the solid matrix of the sponge (the cellulose material itself). Here, K_S is assumed to be constant and ϕ_L and ϕ_G are the liquid and gas porosities, respectively. Those porosities are Eulerian variables, i.e., variables which are defined with respect to the actual state. We can also introduce a total Eulerian porosity ϕ. Starting from the definition of the Eulerian porosity $\phi = V_P/V$ (where V_P is the actual porous volume) and differentiating it, one can link the Eulerian porosity to the Lagrangian one

$$d\phi = d\varphi - \phi d\varepsilon \tag{8}$$

The preceding formula not only holds for the Eulerian total porosity ϕ, but also for the Eulerian gas porosity ϕ_G and for the Eulerian liquid porosity ϕ_L.

Upon drying, the larger pores will empty first. At a given stage of the drying process, the larger pores will be full of gas, while the smaller pores will be full of liquid. In order to characterize the saturation, we introduce a Lagrangian liquid saturation S_L, defined as the pore volume fraction which the saturated pores were occupying *in the undeformed state of reference*.

We assume that there exists a mesoscopic scale made up of the pores full of liquid and of the solid matrix (see Fig. 4). The mesoscopic bulk and shear moduli at this mesoscopic scale are K_M and G_M, respectively. The sponge is a double-porosity medium and, if we impose a zero pore pressure in the pores full of liquid ($p_L = 0$ in the state equations (2)–(4), we should retrieve regular poroelasticity, from which we obtain the following mesoscopic relations

$$b_G = 1 - \frac{K}{K_M} \tag{9}$$

$$\frac{1}{N_{GG}} = \frac{b_G - \phi_G}{K_M} \tag{10}$$

3.2 Shrinkage Properties. We consider a drying sponge subjected to no external stress ($\sigma = 0$). Upon drying, the capillary pressure $p_c = p_G - p_L$ will increase. We aim to calculate how the sponge shrinks.

Since the gas pressure remains constant and equal to the atmospheric one, the state equations (2)–(4) can be rewritten as

$$0 = Kd\varepsilon + b_L dp_c \tag{11}$$

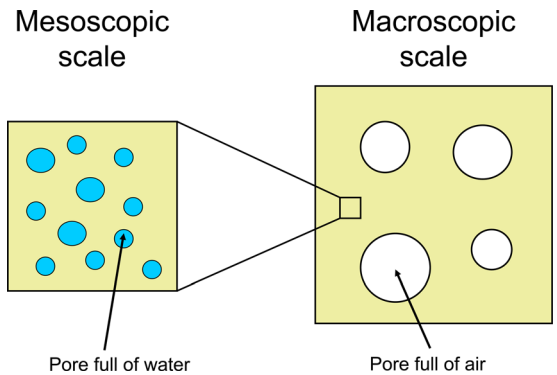

Fig. 4 Two-scale porosity model for a sponge

$$d\varphi_L = b_L d\varepsilon - \frac{dp_c}{N_{LL}} \tag{12}$$

$$d\varphi_G = b_G d\varepsilon - \frac{dp_c}{N_{LG}} \tag{13}$$

As expected, a buildup of capillary pressure leads to a shrinkage of the sponge.

We aim to compute how the mass and volume are linked. We increase the capillary pressure $p_c = p_G - p_L$ at a given Lagrangian liquid saturation S_L (and, therefore, at a given Lagrangian gas saturation $S_G = 1 - S_L$). Equation (8), applied to the gas porosity and combined with Eqs. (11) and (13), yields

$$d\phi_G = d\varphi_G - \phi_G d\varepsilon = b_G d\varepsilon - \frac{1}{N_{LG}} dp_c - \phi_G d\varepsilon \tag{14}$$

$$= \left(-b_G - \frac{K}{N_{LG} b_L} + \phi_G\right) \frac{b_L}{K} dp_c \tag{15}$$

which, with the help of the poroelastic relations (5), (7), (9), and (10), can be rewritten as

$$d\phi_G = 0 \tag{16}$$

In the absence of any capillary pressure, the sponge is in its reference state and $\phi_G = \phi_{G0} = \phi_0(1 - S_L)$. Therefore, an integration of the preceding equation yields

$$\phi_G = \phi_{G0} = \phi_0(1 - S_L) \tag{17}$$

Independently of the capillary pressure, if the Lagrangian liquid saturation remains constant, the Eulerian gas porosity remains constant.

In contrast, Eq. (8), applied to the liquid porosity and combined with Eqs. (11) and (12), yields how the Eulerian liquid porosity varies upon drying

$$d\phi_L = d\varphi_L - \phi_L d\varepsilon = -\left(\frac{b_L^2}{K} - \frac{b_L \phi_L}{K} + \frac{1}{N_{LL}}\right) dp_c \tag{18}$$

$$= -\left[\frac{b_L - \phi_L}{K_M} + \left(\frac{1}{K_M} - \frac{1}{K_S}\right)(b_G - \phi_G)\right] dp_c \tag{19}$$

$$= -\left[\frac{1 - \phi_L - \phi_G}{K_M} - \frac{1 - \phi_G}{K_S}\right] dp_c \tag{20}$$

We use classical micromechanical relations adapted to porous materials with spherical voids (the Mori–Tanaka scheme) to link the mesoscopic bulk modulus with the microporosity and the solid matrix elastic properties [20]. Noting that the liquid porosity, with respect to the mesoscopic volume, is $\phi_L/(1 - \phi_G)$, we find [20]

$$K_M = K_S \frac{4G_S(1 - \phi_L/(1 - \phi_G))}{3K_S(\phi_L/(1 - \phi_G)) + 4G_S} \tag{21}$$

$$= \frac{4G_S}{3} \frac{1 - \phi_L - \phi_G}{\phi_L + 4G_S(1 - \phi_G)/3K_S} \tag{22}$$

so that, eventually, Eq. (20) can be rewritten as

$$d\phi_L = -\frac{3\phi_L}{4G_S} dp_c \tag{23}$$

which can readily be integrated

$$\phi_L = S_L \phi_0 e^{-3p_c/4G_S} \tag{24}$$

The volume strain can be expressed from Eq. (11)

$$d\varepsilon = -\frac{b_L}{K}dp_c = \frac{4G_S}{3\phi_L}\frac{b_L}{K}d\phi_L \tag{25}$$

$$= \left(1+\frac{4G_S}{3K_S}\right)\frac{d\phi_L}{1-\phi_G-\phi_L} \tag{26}$$

Recalling that ϕ_G is constant (see Eq. (17)), the previous equation can readily be integrated

$$V = V_0\left(\frac{1-\phi_0(1-S_L)-\phi_L}{1-\phi_0}\right)^{-(1+4G_S/3K_S)} \tag{27}$$

where V_0 is the volume of the sponge in the reference (wet) state, or, equivalently

$$\phi_L = 1-\phi_0(1-S_L)-(1-\phi_0)\left(\frac{V}{V_0}\right)^{-(1/(1+4G_S/3K_S))} \tag{28}$$

Finally, we can explicitly link the volume V of the sponge to its mass M. The mass of the sponge is the sum of its solid mass M_S and of the mass of water it contains

$$M = M_S + \rho_w V\phi_L = M_S + \rho_w(1-\phi_0(1-S_L))[V-cV^{\alpha}] \tag{29}$$

where

$$c = \frac{1-\phi_0}{1-\phi_0(1-S_L)}V_0^{1/(1+4G_S/3K_S)} \tag{30}$$

$$\alpha = \frac{1}{1+3K_S/4G_S} \tag{31}$$

3.3 Stiffening Properties. We now aim to calculate how the sponge stiffens upon drying. In order to do so, we will use micromechanical relations which enable us to link the macroscopic moduli (K^{mac}, G^{mac}) to the microscopic ones (K^{mic}, G^{mic}) through the porosity $\tilde{\phi}$ of the medium in the case of spherical pores (the Mori–Tanaka scheme) [20]

$$K^{\text{mac}} = K^{\text{mic}}\frac{4(1-\tilde{\phi})G^{\text{mic}}}{3\tilde{\phi}K^{\text{mic}}+4G^{\text{mic}}} \tag{32}$$

$$G^{\text{mac}} = G^{\text{mic}}\frac{(1-\tilde{\phi})(9K^{\text{mic}}+8G^{\text{mic}})}{9K^{\text{mic}}\left(1+\frac{2\tilde{\phi}}{3}\right)+8G^{\text{mic}}\left(1+\frac{3\tilde{\phi}}{2}\right)} \tag{33}$$

The homogenization of the mechanical properties of the sponge is performed in two steps. First, the mesoscopic moduli K_M and G_M are linked to the solid matrix properties K_S and G_S by considering $K^{\text{mac}} = K_M$, $G^{\text{mac}} = G_M$, $K^{\text{mic}} = K_S$, $G^{\text{mic}} = G_S$ and $\tilde{\phi} = \phi_L/(1-\phi_G)$ in Eqs. (32) and (33)

$$K_M = K_S\frac{4(1-\phi_{G0}-\phi_L)G_S}{3\phi_L K_S+4(1-\phi_{G0})G_S} \tag{34}$$

$$G_M = G_S\frac{(1-\phi_{G0}-\phi_L)(9K_S+8G_S)}{9K_S(1-\phi_{G0}+2\phi_L/3)+8G_S(1-\phi_{G0}+3\phi_L/2)} \tag{35}$$

The macroscopic bulk modulus K of the sponge is then calculated by considering $K^{\text{mac}} = K$, $K^{\text{mic}} = K_M$, $G^{\text{mic}} = G_M$, and $\phi = \phi_G$ in Eq. (32)

$$K = \frac{(1-\phi_{G0})K_M}{1+3\phi_{G0}K_M/4G_M} \tag{36}$$

where

$$\frac{K_M}{G_M} = \frac{4K_S}{9K_S+8G_S}\frac{9K_S\left(1-\phi_{G0}+\frac{2\phi_L}{3}\right)+8G_S\left(1-\phi_{G0}+\frac{3\phi_L}{2}\right)}{3\phi_L K_S+4(1-\phi_{G0})G_S} \tag{37}$$

By knowing the elastic properties of the solid matrix, the gas porosity (from Eq. (17)), and the liquid porosity (from Eq. (28)), the preceding equations enable us to calculate the macroscopic bulk modulus K of the sponge.

4 Validation of the Poromechanical Model With the Experimental Results

We now aim to validate the poromechanical model developed in Sec. 3 with the experimental results obtained in Sec. 2. The validation is performed in two steps. First, the poromechanical model is calibrated on the shrinkage data (see Fig. 1). Then the calibrated poromechanical model is compared with the stiffening data (see Fig. 2).

4.1 Shrinkage Properties. The poromechanical model gives us access to the shrinkage behavior of the sponge. Equation (27) shows that the mass M of the sponge depends on its dry mass M_S, on its volume V, on its wet volume V_0, on the mass density ρ_w of water, on the Lagrangian liquid saturation S_L, and on an elastic property K_S/G_S. The dry mass of the sponge is known ($M_S = 23.7$ g; see Sec. 2), as are also known its wet volume ($V_0 = 744$ cm^3; see Sec. 2) and the mass density of water ($\rho_w = 1000$ kg/m^3). Physics tells us that the Lagrangian liquid saturation depends on the capillary pressure [17] or, equivalently, on the volume of the sponge.

Equation (29) was fitted to the experimental data. The best fit is displayed in Fig. 5. This best fit was obtained for $\phi_0 = 98.2\%$, for a diverging elastic property $K_S/G_S \to +\infty$, and for a given function $S_L(V)$. The fact that ϕ_0 was nearly equal to unity shows that a sponge is mostly made of voids, which explains why a sponge can suck up so much water. The fact that K_S/G_S diverged means that the solid matrix of the sponge can be considered as incompressible. In such a case, Eqs. (27) and (29) simplify to

$$V = \frac{(1-\phi_0)V_0}{1-\phi_0(1-S_L)-\phi_L} \tag{38}$$

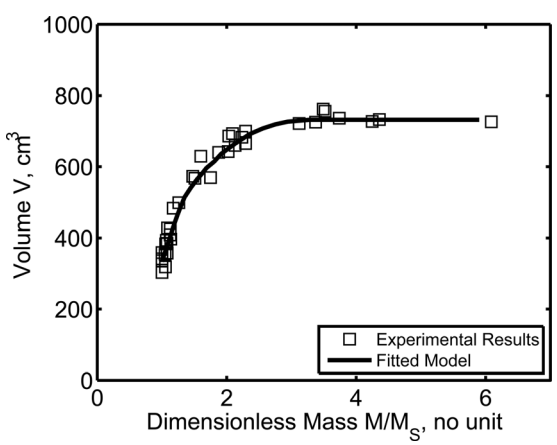

Fig. 5 Volume V of the sponge versus its dimensionless mass M/M_S

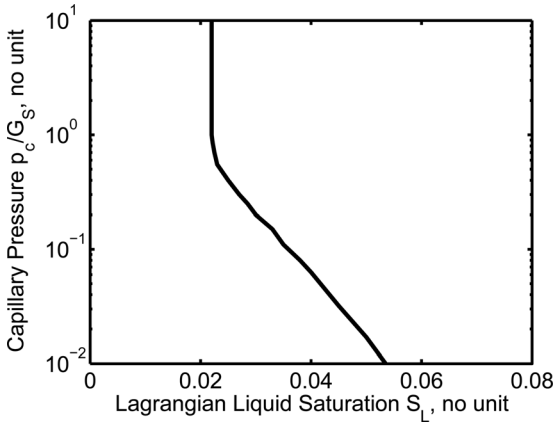

Fig. 6 Retention curve of the sponge: the dimensionless capillary pressure p_c/G_S versus the Lagrangian liquid saturation S_L

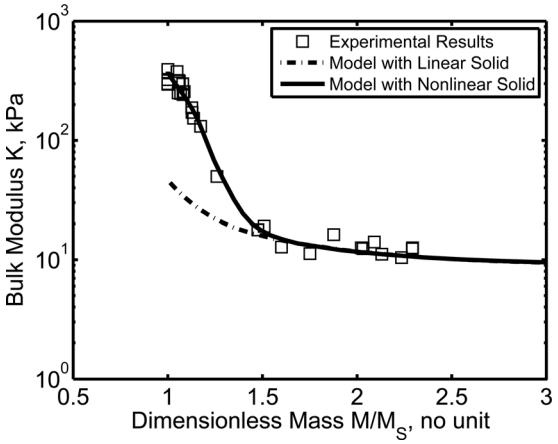

Fig. 7 Bulk modulus K of the sponge versus its dimensionless mass M/M_S

$$M = M_S + \rho_w[(1-\phi_0(1-S_L))V - (1-\phi_0)V_0] \tag{39}$$

Since the volume V of the sponge depends on the liquid porosity ϕ_L, and since this liquid porosity depends on a dimensionless capillary pressure p_c/G_S (see Eq. (24)), the Lagrangian liquid saturation $S_L(V)$ obtained from the fitting of the shrinkage data can also be expressed as a function of this dimensionless capillary pressure just introduced. This function $S_L(p_c/G_S)$, known as the retention curve of the sponge, is displayed in Fig. 6.

Upon drying, the Lagrangian liquid saturation decreased from unity. The retention curve displayed in Fig. 6 shows that, as long as $S_L > 5\%$, the capillary pressure remained negligible with respect to the elastic properties of the solid, which explains why the sponge did not shrink. When drying further ($S_L < 5\%$), the capillary pressure became significant and shrinkage was observed. Interestingly, for the greater capillary pressures ($p_c/G_S > 0.5$), the Lagrangian liquid saturation remained constant. Coming back to the very definition of Lagrangian saturation, such an observation means that pores that were still saturated at low water contents remained saturated even when they further lost water. In other words, in the smallest pores, a loss of water translated into a reduction of pore volume, but did not translate into a desaturation.

4.2 Stiffening Properties. Having identified that the solid matrix of the sponge is mostly incompressible ($K_S/G_S \gg 1$), the micromechanical relations derived in Sec. 3.3 simplify to

$$K_M = G_S \frac{4(1-\phi_{G0}-\phi_L)}{3\phi_L} \tag{40}$$

$$G_M = G_S \frac{1-\phi_{G0}-\phi_L}{1-\phi_{G0}+2\phi_L/3} \tag{41}$$

$$K = G_S \frac{4(1-\phi_{G0})(1-\phi_{G0}-\phi_L)}{3\phi_L + 3\phi_{G0}(1-\phi_{G0}+2\phi_L/3)} \tag{42}$$

$$G = G_M \frac{(1-\phi_{G0})(8+9K_M/G_M)}{8(1+3\phi_{G0}/2)+9(1+2\phi_{G0}/3)K_M/G_M} \tag{43}$$

A calculation of Poisson's ratio $\nu = (3K-2G)/2(3K+G)$ with the calibrated poroelastic parameters yields that, upon drying, Poisson's ratio varies between 0.24 and 0.31, thus validating the assumption $\nu = 0.25$ made in Sec. 2.1.

We infer from Eq. (43) that $K = G_S\tilde{K}(\phi_{G0}, \phi_L)$, where all parameters of the dimensionless bulk modulus $\tilde{K}$ are accessible from the calibration performed in Sec. 4.1. Therefore, based on the calibrated poromechanical model, the bulk modulus of the sponge must be known, close to a proportionality factor (the shear modulus G_S of the solid matrix).

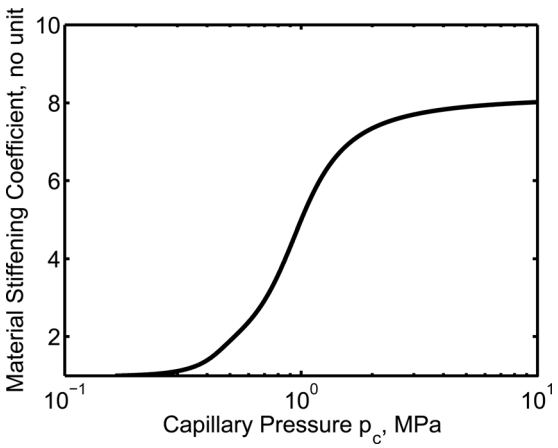

Fig. 8 Material stiffening of the sponge. The material stiffening coefficient is defined as $G_S(p_c)/G_S(p_c = 0)$.

Equation (43), for $G_S = 0.85$ MPa, is displayed in Fig. 7, together with the experimental data of stiffening upon drying. We observe that the poromechanical model developed here can only partially explain the stiffening induced by drying. Indeed, upon drying, the bulk modulus of the sponge increased by about 1.5 orders of magnitude, while our poromechanical model only explains about half of this increase. Therefore, the stiffening of the cellulose sponge upon drying is partly explained by the closing of the pores under the action of capillary pressure.

The poromechanical model we developed is based on the assumption that the solid matrix is linear elastic. However, it may be that the solid matrix behaves nonlinearly. In such a case, the elastic moduli would depend on the effective stress. For a drying sponge, the effective stress at the mesoscopic scale is equal to the capillary pressure p_c. By introducing material nonlinearities of the solid matrix, it is possible to fully capture the stiffening behavior of the sponge, as can be observed in Fig. 7. The nonlinear elastic behavior of the solid matrix that enables us to capture the stiffening of the sponge for the whole range of water contents is displayed in Fig. 8 by using a 'material stiffening factor,' defined as $G_S(p_c)/G_S(p_c = 0)$. This material stiffening of the cellulose matrix itself could be due to the creation of additional hydrogen bonds between neighboring chains of cellulose. Such a stiffening could also be due to the microporous nature of the cellulose

matrix, since we know that the adsorption of fluid in microporous solids can induce apparent mechanical nonlinearities [21].

5 Conclusions

In this work, we measured and modeled how a sponge shrinks and stiffens upon drying. In order to explain the experimental observations, we developed a partially-saturated poromechanical model based on the Biot–Coussy framework in finite transformations.

The poromechanical model enabled us to capture the shrinkage of the sponge, experimentally observed for the whole range of water contents. The retention curve of the sponge was back-calculated. At the highest capillary pressures, pores that were saturated remained saturated, even when further drying was applied: in the smallest pores a loss of water translated into a reduction of the pore volume, but did not translate into further desaturation.

The poromechanical model could partially capture the stiffening of the sponge experimentally observed upon drying. Part of this stiffening could be explained by the closing of the pores under the action of capillary pressure. The model nevertheless underestimated the observed stiffening: the cellulose matrix of the sponge may behave nonlinearly because of the creation of additional hydrogen bonds between neighboring cellulose chains or because of its microporous nature.

Acknowledgment

Our thoughts go to the late Professor Olivier Coussy, who inspired this study. He is missed and remembered as a friend and as a mentor.

Nomenclature

b_G = Biot coefficient of the sponge associated to the gas phase
b_L = Biot coefficient of the sponge associated to the liquid phase
E_i = Young's modulus of the sponge in the ith direction
G = shear modulus of the sponge
G_M = mesoscopic shear modulus
G_S = shear modulus of the solid matrix of the sponge
K = bulk modulus of the sponge
K_M = mesoscopic bulk modulus
K_S = bulk modulus of the solid matrix of the sponge
M = mass of the sponge
N_{GG} = first Biot modulus of the sponge
N_{LG} = second Biot modulus of the sponge
N_{LL} = third Biot modulus of the sponge
p_c = capillary pressure
p_G = pressure of the gas phase
p_L = pressure of the liquid phase
S_G = Lagrangian gas saturation
S_L = Lagrangian liquid saturation
V = volume of the sponge
V_P = porous volume of the sponge
ε = volumetric strain
ν = Poisson's ratio of the sponge
ρ_w = mass density of water
σ = volumetric part of the confining stress
ϕ = Eulerian total porosity
ϕ_G = Eulerian gas porosity
ϕ_{G0} = gas porosity in the state of reference
ϕ_L = Eulerian liquid porosity
ϕ_{L0} = liquid porosity in the state of reference
ϕ_0 = total porosity in the state of reference
φ = variation of the porosity
φ_G = variation of the porosity occupied by the gas phase
φ_L = variation of the porosity occupied by the liquid phase

References

[1] O'Sullivan, A. C., 1997, "Cellulose: The Structure Slowly Unravels," Cellulose, **4**(3), pp. 173–207.
[2] Purves, C. B., 1954, *Chain Structure in Cellulose and Cellulose Derivatives: Part 1*, Wiley-Interscience, New York.
[3] Sjöström, E., 1981, *Wood Chemistry Fundamentals and Applications*, Academic, New York.
[4] Tashiro, K., and Kobayashi, M., 1991, "Theoretical Evaluation of Three-Dimensional Elastic Constants of Native and Regenerated Celluloses: Role of Hydrogen Bonds," Polymer, **32**(8), pp. 1516–1526.
[5] Hinterstoisser, B., Akerholm, M., and Salmén, L., 2001, "Effect of Fiber Orientation in Dynamic FTIR Study on Native Cellulose," Carbohydr. Res., **334**(1), Aug., pp. 27–37.
[6] Akerholm, M., Hinterstoisser, B., and Salmén, L., 2004, "Characterization of the Crystalline Structure of Cellulose Using Static and Dynamic FT-IR Spectroscopy," Carbohydr. Res., **339**(3), pp. 569–578.
[7] Tanaka, F., and Fukui, N., 2004, "The Behavior of Cellulose Molecules in Aqueous Environments," Cellulose, **11**(1), pp. 33–38.
[8] Luukko, K., and Maloney, T. C., 1999, "Swelling of Mechanical Pulp Fines," Cellulose, **6**(2), pp. 123–135.
[9] Scallan, A. M., and Grignon, J., 1979, "Effect of Cations on Pulp and Paper Properties," Svensk Papperstidning-nordisk Cellulosa, **82**(2), pp. 40–47.
[10] Lindström, T., and Carlsson, G., 1982, "The Effect of Chemical Environment on Fiber Swelling," Svensk Papperstidning-nordisk Cellulosa, **85**, pp. R14–R20.
[11] Scallan, A. M., and Tigerström, A. C., 1992, "Swelling and Elasticity of the Cell-Walls of Pulp Fibers," J. Pulp Pap. Sci., **18**(5), pp. J188–J193.
[12] Sahin, H. T., and Arslan, M. B., 2008, "A Study on Physical and Chemical Properties of Cellulose Paper Immersed in Various Solvent Mixtures," Int. J. Mol. Sci., **9**(1), pp. 78–88.
[13] Hofstetter, K., Hinterstoisser, B., and Salmén, L., 2006, "Moisture Uptake in Native Cellulose—The Roles of Different Hydrogen Bonds: A Dynamic FT-IR Study Using Deuterium Exchange," Cellulose, **13**(2), pp. 131–145.
[14] Hatakeyama, H., and Hatakeyama, T., 1998, "Interaction Between Water and Hydrophilic Polymers," Thermochim. Acta, **308**(1–2), pp. 3–22.
[15] Eichhorn, S. J., Baillie, C. A., Zafeiropoulos, N., Mwaikambo, L. Y., Ansell, M. P., Dufresne, A., Entwistle, K. M., Herrera-Franco, P. J., Escamilla, G. C., Groom, L., Hughes, M., Hill, C., Rials, T. G., and Wild, P. M., 2001, "Review: Current International Research Into Cellulosic Fibres and Composites," J. Mater. Sci., **36**(9), pp. 2107–2131.
[16] Myllytie, P., Salmén, L., Haimi, E., and Laine, J., 2009, "Viscoelasticity and Water Plasticization of Polymer-Cellulose Composite Films and Paper Sheets," Cellulose, **17**(2), pp. 375–385.
[17] Coussy, O., 2010, *Mechanics and Physics of Porous Solids*, Wiley, New York.
[18] Wittman, F., 1968, "Surface Tension, Shrinkage and Strength of Hardened Cement Paste," Mater. Struct. (in French: Matériaux et Constructions), **1**(6), pp. 547–552.
[19] Coussy, O., 2004, *Poromechanics*, Wiley, New York.
[20] Dormieux, L., Kondo, D., and Ulm, F.-J., 2006, *Microporomechanics*, Wiley, New York.
[21] Brochard, L., Vandamme, M., and Pellenq, R.-M., 2012, "Poromechanics of Microporous Media," J. Mech. Phys. Solids, **60**(4), pp. 606–622.